Analysis of Common-Mode Noise for Weakly Coupled Differential Serpentine Delay Microstrip Line in High-Speed Digital Circuits

Guang-Hwa Shiue, *Member, IEEE*, Jia-Hung Shiu, Yi-Chin Tsai, and Che-Ming Hsu

***Abstract*—This study investigates the mechanisms of generation of the transient transmission common-mode noise in a differential serpentine delay line under weak coupling condition. The generation mechanism and the frequency of common-mode noise are investigated with reference to the time-domain transmission waveform and the differential-to-common mode conversion mixed-mode *S*-parameters using the circuit solver HSPICE and 3-D full-wave simulator HFSS, respectively. The generation mechanisms of common-mode noise include length mismatch between vertical-turn-coupled traces, the length effect of parallel-coupled traces, and the crosstalk noise effect. Moreover, a graphical method based on wave tracing is presented to illustrate the cancellation mechanism of near-end common-mode noise for the symmetrical differential serpentine delay line. Some practical, commonly used layout routings of the differential serpentine delay line are investigated. Some important design guidelines are provided to help design differential serpentine delay line with low common-mode noise. A comparison between simulated and measured results validates the equivalent circuit model and analytical approach.**

***Index Terms*—Common-mode noise, crosstalk noise, differential serpentine delay line, differential-to-common mode conversion, length mismatch, mixed *S*-parameter.**

I. Introduction

As the clock frequencies and data transmission rates in semiconductor systems steadily increase into the gigahertz range, timing control of the high-speed clock and digital data signal traces on printed circuit board (PCB) and packages becomes critical to the design of high-speed digital circuits. While many approaches for minimizing clock or digital data signal skew have been presented, delay lines are generally adopted in the critical nets of a PCB, as in the serpentine routing scheme, which is shown in Fig. 1.

Differential transmission lines are gradually becoming more common than single transmission lines for routing in modern high-speed digital circuits, such as PCBs and packages, because they suffer less from interference than does a single transmission line [1]. Notable applications include the serial advanced technology attachment III (6 Gbps), the high-definition multimedia interface (5 Gbps), the PCI express interconnect (8 Gbps), and USB 3.0 (5 Gbps) devices. Since such high-speed digital systems comprise multiple differential interconnects, timing synchronization is a serious design issue. Hence, the serpentine delay line has recently been employed to pass differential signals, serving as a differential serpentine delay line. Intuitively, the total time delay should be proportional to the total length of the differential serpentine delay line. However, the crosstalk noise that is induced by close differential line pairs sections may drastically worsen the total time delay and even result in the false switching of logic gates. Therefore, the crosstalk mechanism in differential serpentine delay line has been investigated [2]–[4].

Differential signals transmission ideally maintains good signal integrity and exhibits low electromagnetic emission or electromagnetic interference. However, in practical circuits, the differential signal pairs may accompany unwanted common-mode noise when the differential signals are skewed in time (as when differential traces exhibit a length mismatch), coupled crosstalk noise, and other effects. Owing to the differential serpentine scheme, the differential serpentine delay line is always associated with unwanted common-mode noise. In high-speed data links, cables are always required to transmit differential signals between electronic devices. The common-mode noise may couple to the I/O cables and form an excitation source of

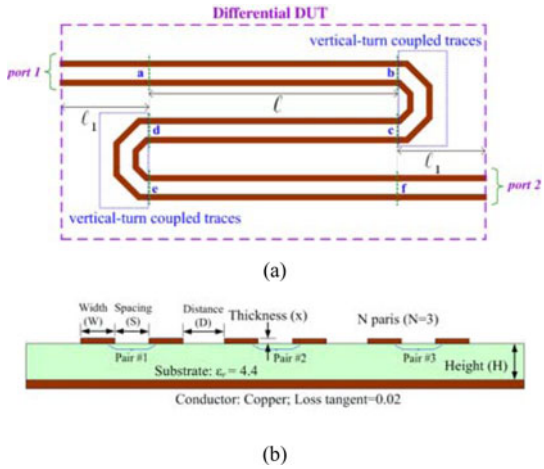

Fig. 1. (a) Top view and (b) cross-sectional views of the differential serpentine delay lines in a microstrip structure (for $N = 3$).

Manuscript received June 25, 2011; revised September 16, 2011; accepted October 20, 2011. Date of publication November 21, 2011; date of current version June 15, 2012. This work was supported in part by the National Science Council, Republic of China under Grant NSC 98/99-2221-E-033-014, in part by the College of Electrical Engineering and Computer Science under Grant CYCU-EECS-9903, and in part by Inventec under Grant 1000910.

The authors are with the Department of Electronic Engineering, Chung Yuan Christian University, Taoyuan 22065, Taiwan (e-mail: ghs.apemc@msa.hinet.net; gahong94@cycu.org.tw; chin70229@gmail.com; cmhsu@cycu.org.tw).

Color versions of one or more of the figures in this paper are available online at http://ieeexplore.ieee.org.

Digital Object Identifier 10.1109/TEMC.2011.2173765

the antenna [5]. However, the previous studies have focused on the crosstalk effect, transient waveforms, and the phase-delay time [6] for differential serpentine delay line. Common-mode noise on a differential serpentine delay line has not been investigated.

This paper investigates the mechanism of generation of transient transmission common-mode noise in a differential serpentine delay line under weakly coupled condition. The time-domain transient waveforms of generation mechanisms are simulated by HSPICE. The mechanisms are validated in the time domain using the 3-D full-wave simulator, CST [7]. Additionally, the differential-to-common mode conversion S_{c2d1} mixed-mode S-parameters [8] are used to verify the time-domain simulation results obtained using the HFSS [9].

This paper is organized as follows. In Section II, the circuit model for a differential serpentine delay line is constructed and the problem of interest is described. Section III investigates the mechanisms of generation of common-mode noise in a differential serpentine delay line. Subsequently, the cancellation mechanism of near-end common-mode noise for a symmetrical differential serpentine delay line structure is explained using a graphical method. Section IV focuses on the common-mode noise of some practical layout routings. Important guidelines for designing a differential serpentine delay line are presented. Section V compares simulated and measured results for verification purposes, and Section VI draws brief conclusions.

II. Statement of the Problem and Circuit Modeling

Fig. 1 shows a typical differential serpentine delay line that is formed by coupled microstrip lines with three parallel differential trace pairs. Fig. 1 presents the top and cross-sectional views of the differential serpentine delay line, specifying all structural parameters, such as line width W of differential traces, length ℓ of parallel-coupled traces, length ℓ_1 of parallel-coupled traces that are connected to port, the height H of the substrate, the dielectric constant ε_r of the substrate, the thickness x of the signal trace, the spacing D between differential trace pairs, the distance S between differential traces, and the number N of section in a differential serpentine traces.

An ideal differential interconnect of a serial link maintains differential symmetry, such that common-mode noise is not an issue. However, in a microstrip differential serpentine delay line, some issues concerning common-mode noise at the receiving end arise. These concern the differential bends, the length of the parallel differential traces, the crosstalk effect in parallel differential trace pairs, asymmetric structure, and others. Fig. 1(a) shows two differential vertical-turn-coupled traces, each with four differential bends in a differential serpentine delay line for $N = 3$. The asymmetries of the differential vertical-turn-coupled traces involve mismatching trace lengths and bent discontinuities. These two asymmetries can result in common-mode noise [11]. Moreover, the crosstalk noise effect between differential line pairs in a compact situation also produces common-mode noise. Like the dual back-to-back-coupled bends effect [11] in differential interconnects, the reduction of common-mode noise associated with the dual back-to-back vertical-turn-coupled traces must also be investigated.

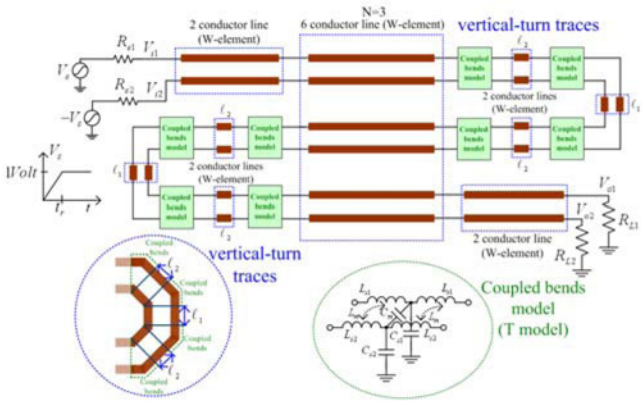

Fig. 2. Graphical configuration of the simulation method used in HSPICE for a differential serpentine delay line (for $N = 3$).

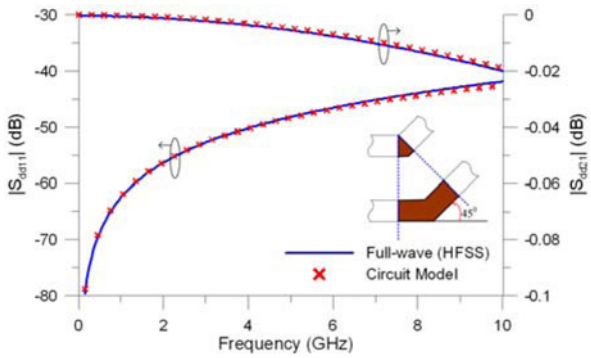

Fig. 3. Comparison of the simulation results of differential reflection and insertion losses of 45° angle coupled bends between the equivalent circuit model and full-wave simulator (HFSS).

Fig. 2 presents the circuit model that is used in the HSPICE simulation of the differential serpentine delay line with $N = 3$. The multiple-coupled transmission lines are modeled using W-elements, thereby taking into account the finite transmission line loss. The coupled and single transmission lines of vertical-turn traces are also modeled using W-elements. The figure also presents the T model of the 45° angle coupled bends [10]. The extracted parameters [11] of the coupled bends model are $L_{s1} = 1.23 \times 10^{-2}$ nH, $L_{s2} = 7.175 \times 10^{-2}$ nH, $L_m = 3.5 \times 10^{-3}$ nH, $C_{s1} = 7.8 \times 10^{-3}$ pF, $C_{s2} = 4.3 \times 10^{-2}$ pF, and $C_m = 0.5 \times 10^{-3}$ pF. In addition, Fig. 3 shows the comparison of the simulation results of differential reflection and insertion losses of the coupled bends between the equivalent circuit model and full-wave simulator (HFSS). The favorable comparison validates the proposed equivalent circuit model of 45° angle coupled bends. For simplicity, the differential sources are ideal symmetric. Common-mode noise does not exist at the driving sources of the differential serpentine delay line.

In this study, for time-domain analysis, the common-mode voltage V_c and differential-mode voltage V_d are, respectively, defined by

$$V_{c,i} = \frac{V_{1,i} + V_{2,i}}{2} \tag{1a}$$

$$V_{d,i} = V_{1,i} - V_{2,i} \tag{1b}$$

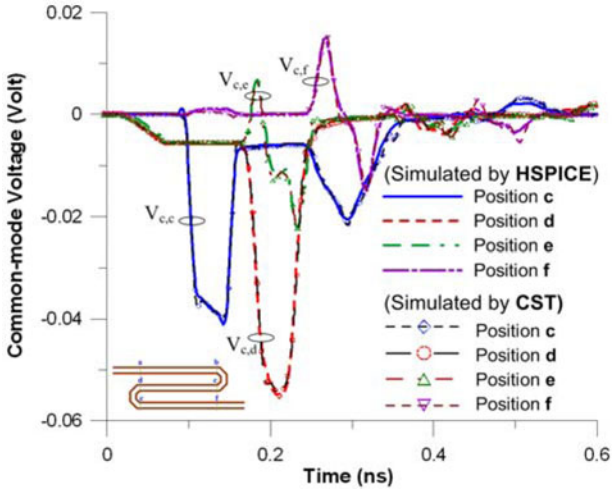

Fig. 4. Comparison of simulated transient transmission common-mode voltages between HSPICE and CST on a differential serpentine delay line.

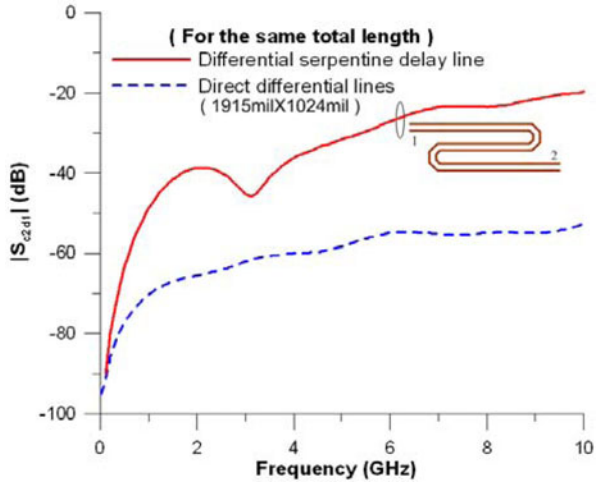

Fig. 5. Comparison of simulated differential-to-common mode conversions between a differential serpentine delay line ($N = 3$) and direct differential lines for the same total length.

where $V_{1,i}$ and $V_{2,i}$ denote the two voltages on the two differential lines, respectively, at the same vertical position relative to the differential serpentine delay line. The subscript "*i*" denotes the position—a, b, c, d, e, and f—on the differential serpentine delay line, as shown in Fig. 1(a).

The mechanism of generation of common-mode noise investigated using the transient waveform in the time-domain and the frequency-domain validation is also presented. Accordingly, the mixed-mode *S*-parameters [8] are widely adopted to perform the differential interconnects, such as differential serpentine delay microstrip line in frequency-domain analysis. A two-port differential device under test, differential serpentine delay microstrip line, is also shown in Fig. 2(a). A matrix of mixed-mode *S*-parameters can be constructed in a way similar to the single-ended traditional *S*-parameters matrix as

$$[S]_{4\times4} = \begin{bmatrix} S_{d1d1} & S_{d1d2} & S_{d1c1} & S_{d1c2} \\ S_{d2d1} & S_{d2d2} & S_{d2c1} & S_{d2c2} \\ S_{c1d1} & S_{c1d2} & S_{c1c1} & S_{c1c2} \\ S_{c2d1} & S_{c2d2} & S_{c2c1} & S_{c2c2} \end{bmatrix} = \begin{bmatrix} [S_{dd}] & [S_{dc}] \\ [S_{cd}] & [S_{cc}] \end{bmatrix} \quad (2)$$

where S_{didj} and S_{cicj} $(i, j = 1, 2)$ are the differential-mode and common-mode *S*-parameters, respectively. S_{dicj} and S_{cidj} $(i, j = 1, 2)$ are the mode-conversion *S*-parameters. For a differential serpentine delay microstrip line, the differential-to-common mode conversion S_{c2d1} is selected to characterize common-mode noise at the reviving end in the frequency domain.

Consider a practical routing differential serpentine delay line in mile-scale industrial PCB, as shown in Fig. 2(a). Fig. 2(b) shows the cross-sectional view that corresponds to Fig. 2(a), with $W = 7.5$ mil, $S = 9.5$ mil, $H = 5.5$ mil, $D = 17$ mil, $x = 1.7$ mil, $\varepsilon_r = 4.4$, loss tangent $= 0.02$, $\ell_1 = 102$ mil, and $\ell = 536$ mil. The driving sources are a ramp pulse with a magnitude of $\pm$ 0.5 V and a rise time t_r of 50 ps. The driver and load resistance are chosen as $R_{s1} = R_{s2} = R_{L1} = R_{L2} = 50\ \Omega$. The differential impedance is about 100 Ω (i.e., the odd impedance is about 50 Ω) and the coupling coefficient [12] of the coupled microstrip lines is about 0.1. Therefore, the differential traces of the differential serpentine delay line are weakly coupled.

Fig. 4 compares the transient transmission common-mode voltages simulated using HSPICE and CST for a differential serpentine delay line. Clearly, the results simulated using HSPICE are consistent with those obtained using the CST. At the internal positions, c and d, the common-mode voltage has the large amplitude. Furthermore, the common-mode voltages at positions c, d, and e have a flat dc voltage component. However, the common-mode voltage at the relative receiving position f does not have a large flat dc voltage component. Therefore, the large flat dc component of the common-mode voltage within the differential serpentine delay line is almost entirely absent at the receiving end.

Fig. 5 compares the differential-to-common mode conversion that was simulated by HFSS for a differential serpentine delay line ($N = 3$) with that for direct differential lines with the same total length. Clearly, the differential serpentine delay line exhibits larger differential-to-common mode conversion over a wide range of frequencies. Restated, the common-mode noise is larger at the receiving end when the differential signals pass through the differential serpentine delay line than when they pass through the direct differential lines. The corresponding differential-to-common mode conversion for a differential serpentine delay line with $N = 3$ is $V_{c,f}$, as shown in Fig. 4. Notably, although the direct differential lines have a perfectly symmetrical structure, a slight differential-to-common mode conversion, shown in Fig. 5, still occur because of the asymmetrical numerical solutions obtained using the 3-D full-wave solver (HFSS) for the two traces of direct differential lines. Most of the asymmetrical solutions are attributable to the asymmetry of the solved meshes [9].

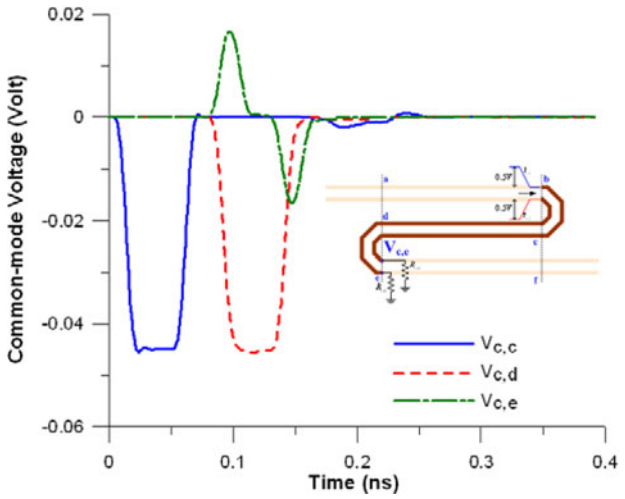

Fig. 6. Comparison of common-mode voltages on the part of the structure of a differential serpentine delay line.

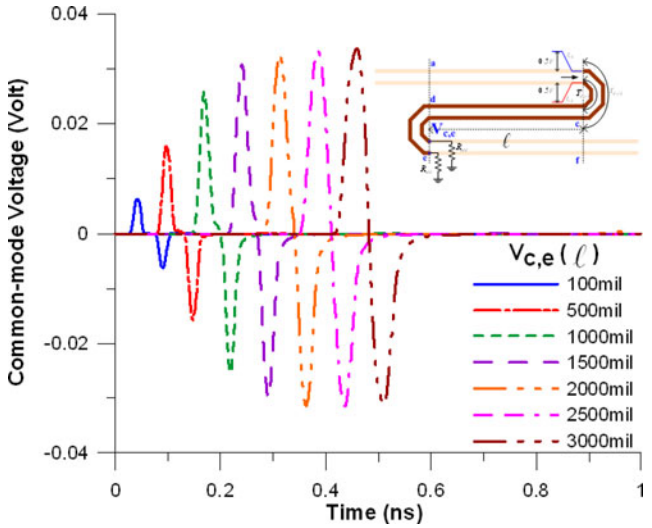

Fig. 7. Remnant common-mode noise of the dual back-to-back vertical-turn-coupled traces of a differential serpentine delay line observed at the position e for various length ℓ.

The general guideline for designing differential serpentine delay lines is to ensure that the trace lengths of the two differential traces are equal. Although the lengths of the two differential traces are equivalent to each other, according to the scheme for routing dual back-to-back vertical-turn-coupled traces, as shown in Fig. 2(a), common-mode noise still is generated at the receiving end. The intense common-mode noises, as presented in Fig. 4, in the interior of the differential serpentine delay line are absent at the receiving end. The following section investigates mechanisms of generation of transient transmission common-mode noise for differential serpentine delay line.

III. Generation Mechanism of Common-Mode Noise for Differential Serpentine Delay Line

A. Length Mismatch of Vertical-turn-Coupled Traces

The same parameters as in the previous example in Section II were used in a simulation structure that includes only two vertical-turn-coupled traces and one pair of differential traces that connected the two vertical traces, as shown in Fig. 6. Therefore, an ideal differential ramped step source with a magnitude of $\pm$ 0.5 V and a rise time of 50 ps is driven at position b. The common-mode voltage $V_{c,c}$ at position c is generated by the mismatch of lengths of the vertical-turn-coupled traces. The amplitude of the common-mode voltage $V_{c,c}$ can be approximated by

$$V_c = \frac{V_{\text{in}}}{t_r}\Delta t_v \tag{3}$$

The term t_v is the time difference between the two time delays of the vertical-turn-coupled traces. The t_v in this example is about 8.2 ps and the amplitude of the common-mode voltage $V_{c,c}$ is about 42 mV, according to (3). Furthermore, a common practical routing scheme, like the dual back-to-back-coupled bends scheme [11], using dual back-to-back vertical-turn-coupled traces that are embedded in a differential serpentine delay lines is employed to maintain the equivalent trace length without the significant skew. Hence, most of the common-mode noise is canceled at position e. However, some noise remains at position e, as shown in Fig. 6. The dual back-to-back vertical-turn-coupled traces of a differential serpentine delay line can eliminate most of the common-mode noise.

B. Length Effect of Parallel-Coupled Traces

Since the velocities of the even-mode and odd-mode signals are equal, the stripline structure can almost cancel the common-mode noise but the microstrip structure cannot for dual back-to-back vertical-turn-coupled traces that are embedded in differential serpentine delay line [11]. With the parameters of the structure used in the previous example, a differential ramped step signal with a magnitude of $\pm$ 0.5 V and a rise time of 50 ps is used for excitation. Consider the dual vertical-turn-coupled traces with various inner lengths $\ell = 100, 500, 1000, 2000, 2500,$ and 3000 mil as a parameter. Although the dual back-to-back vertical-turn-coupled traces can help to reduce the common-mode noise, the remnant common-mode noise at position e for various lengths is as shown in Fig. 7. However, the compensation becomes less effective as the length of the coupled lines between the two vertical-turn-coupled traces increases [11].

As the routing length of the coupled lines between dual back-to-back vertical-turn-coupled traces increases, the difference ($\Delta t = T_{\text{even}} - T_{\text{odd}}$) between the delay times of the odd-mode and even-mode signals that is induced by the first (i.e., right side) differential vertical-turn-coupled traces and the remnant common-mode noise at position e increases. Nonetheless, the remnant common-mode noise increases to become saturate when the difference between the propagation times of the even-mode and odd-mode signals along the length equals twice the difference between the delay times, $2\tau = 2 \times (T_{d,v2} - T_{d,v1})$, of the two vertical-turn-coupled traces. Notably, this difference is the time delay $T_{d,v2}$ observed in the outer vertical-turn trace for the time delay $T_{d,v1}$ in the inner vertical-turn trace, as shown in Fig. 7. After the remnant common-mode noise has reached

the saturation, increasing the length increases the transient width of common-mode noise [11].

With respect to the simulated remnant common-mode noise waveforms with various ℓ, mentioned in the preceding section, the maximum magnitude of the common-mode noise is derived as presented elsewhere [11]. A simple, graphical presentation of the results follows. According to (1), the voltages $(V_{1,i}, V_{2,i})$ on the two differential lines also can be calculated as linear combinations of common-mode and differential-mode voltages

$$V_{1,i} = \frac{2V_{c,i} + V_{d,i}}{2} \tag{4a}$$

$$V_{2,i} = \frac{2V_{c,i} - V_{d,i}}{2}. \tag{4b}$$

Consider an ideal differential ramped step source, with a magnitude of $\pm$ 0.5 V and a rise time t_r, that is driven at position b of the simulated structure in Section III-A. According to (1) and (4), Fig. 8(a) plots the related voltage waveforms at positions b, c, d, and e in the structure. For simplicity, the voltage waveforms in Fig. 8(a) are based on the following assumptions: 1) differential transmission lines are lossless; 2) the coupling between coupled lines is negligible; 3) the discontinuity effect of bends is negligible; and 4) the common propagation time is negligible. Additionally, since the common propagation time is neglected for every signal pair ($V_{1,i}$, $V_{2,i}$ or $V_{d,i}$, $V_{c,i}$), the time of the first arrival at each position is measured from time "0" in Fig. 8(a). Therefore, three signal pairs, $(V_{1,d}, V_{1,e})$, $(V_{2,b}, V_{2,c})$, and $(V_{d,d}, V_{d,c})$, clearly have the same voltage waveforms, which are shown in Fig. 8(a).

From Fig. 8(a), the remnant common-mode noise $V_{c,e}$ at position e is half of the sum of $V_{1,e}(V_{1,d})$ and $V_{2,e}$ ($V_{2,d}$ with delay τ). According to (1) and (4), $V_{c,c}$ and $V_{c,d}$ are linear combinations of $V_{1,c}$ and $V_{2,c}$. Moreover, $V_{c,d}$ and $V_{d,d}$ are linear combinations of $V_{1,d}$ and $V_{2,d}$. Because the waveforms of $V_{2,c}$ and $V_{d,c}$ are the same as those of $V_{2,b}$ and $V_{d,d}$, respectively, the differences between the waveforms of $V_{1,c}$ and $V_{1,d}$ and between those of $V_{2,c}$ and $V_{2,d}$ are the same, and determined by the difference between the waveforms of $V_{c,c}$ and $V_{c,d}$ ($V_{c,c}$ with delay Δt), according to (4). Therefore, $\Delta V_1'$ and $\Delta V_2'$ are defined as the differences obtained by subtracting $V_{1,c}$ from $V_{1,e}$ ($V_{1,d}$) and subtracting $V_{2,b}$ from $V_{2,d}$, respectively. Furthermore, $\Delta V'$ can also be obtained from ($V_{c,d}$- $V_{c,c}$). Consequently, based on the aforementioned analyses, the remnant common-mode noise $V_{c,e}$ can be calculated as half of the sum of $\Delta V_1'$ and $\Delta V_1'$ with delay τ, as shown at the bottom of Fig. 8(a).

The first time difference τ between the vertical-turn traces determines the rise time of the waveform $\Delta V_1'$ ($= V_{c,d}$- $V_{c,c}$). The time difference Δt determines the plus width $(\Delta t + \tau)$ of $\Delta V_1'$. The second time difference τ between the vertical-turn traces is the delay time of $\Delta V_1'$, as shown at the bottom of Fig. 8(a). Accordingly, the remnant common-mode noise $V_{c,e}$ can be regarded as the resultant of two identical trapezoid waveforms with the same rise time τ and plus width $(\Delta t + \tau)$, with a time shift of τ between them.

As determined by the range of Δt, the resultant voltage $V_{c,e}$ can be identified as satisfying one of three conditions, which are $\Delta t < 2\tau$, $\Delta t = 2\tau$, and $\Delta t > 2\tau$. For $\Delta t < 2\tau$, as Δt

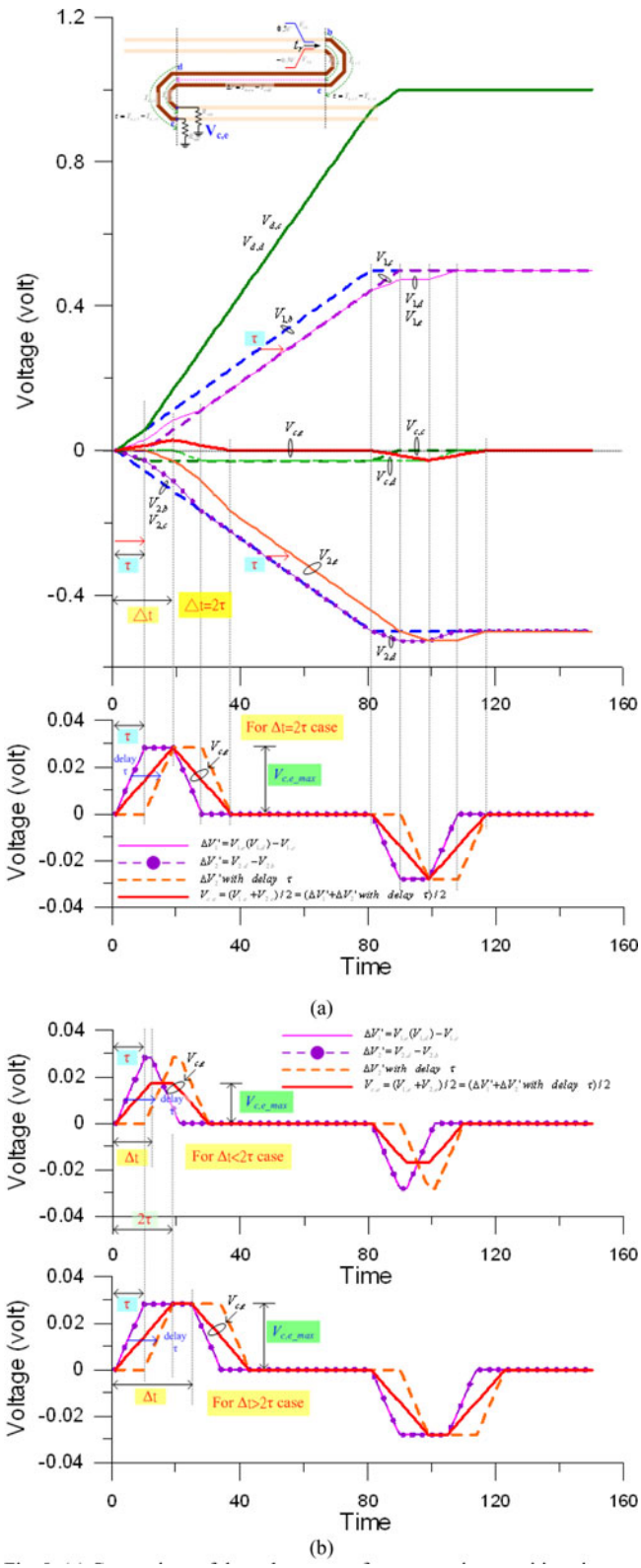

Fig. 8. (a) Comparison of the voltage waveforms at various positions in a dual back-to-back vertical-turn-coupled traces with middle differential lines of a differential serpentine delay line for $\Delta t = 2\tau$ case. (b) Resultant voltage $V_{c,e}$ for $\Delta t < 2\tau$ and $\Delta t > 2\tau$.

TABLE I
COMPARISON OF THE REMNANT COMMON-MODE NOISE AT POSITION E BETWEEN HSPICE SIMULATION AND APPROACH (5)

$V_{c,e}$ (mV)	$\ell = 500$mil	$\ell = 2000$mil
HSPICE Simulation	15.41	35.2/39.8(loss/lossless)
Approach Formula (9)	15.43	41

increases, the maximum magnitude of $V_{c,e}$ increases, as shown in Fig. 8(b). For $\Delta t = 2\tau$, the magnitude of $V_{c,e}$ is at its saturation value, as shown at the bottom of Fig. 8(a). For $\Delta t > 2\tau$, the maximum magnitude of $V_{c,e}$ reaches saturation and an increase in Δt results only in an increase in the pulse width, as shown in Fig. 8(b).

In common case in which $T_{d,v1}$,$T_{d,v2} << t_r$, the maximum coupled noise is approximated by [11]

$$V_{c,e\_\max} = \frac{V_{\text{in}}}{4t_r} \times \min[2\tau, \Delta t] \tag{5}$$

where the time difference $\Delta t = (\ell/v_{\text{even}}) - (\ell/v_{\text{odd}})$is related to the percentage velocity difference

$$\Delta v(\%) = \frac{v_{\text{odd}} - v_{\text{even}}}{v_{\text{average}}} \tag{6}$$

by

$$\Delta t = \frac{\ell}{v_{\text{average}}} \times \Delta v(\%) \tag{7}$$

where v_{even}andv_{odd} are the velocities of the common and differential modes, and $v_{\text{average}}$is their average.

Table I compares the remnant common-mode noises at position e obtained by the HSPICE simulation and using (5). The estimated maximum magnitude of common-mode noise is accurately given by (5). However, in the case of long trace, the magnitude of common-mode noise is slightly degraded due to the loss.

C. Crosstalk Noise Effects

The differential serpentine delay line is formed from coupled microstrip lines, as shown in Fig. 2(a). The near-end crosstalk (NEXT) V_n among the sections of a serpentine delay line is well known to accumulate in phase, appearing as a laddering wave on the time-domain transmission (TDT) waveform [2], [3]. Hence, the concept of trace-to-trace coupling can be utilized to apply the crosstalk-induced single-end delay exactly to the differential serpentine delay line.

Under the assumption of weakly coupling, lossless and matched loads at both ends, the main signal in the active line is weakly influenced by the presence of crosstalk noise. With respect to the ramped step voltage V_i on the active line, the saturated near- and far-end crosstalk voltages (for $tr < 2Td$) in the victim line can be expressed as [13]

$$V_n \approx V_i \times k_{\text{near}} = V_i \times \frac{1}{4}\left(\frac{L_m}{L_s} + \frac{C_m}{C_s + C_m}\right) \tag{8}$$

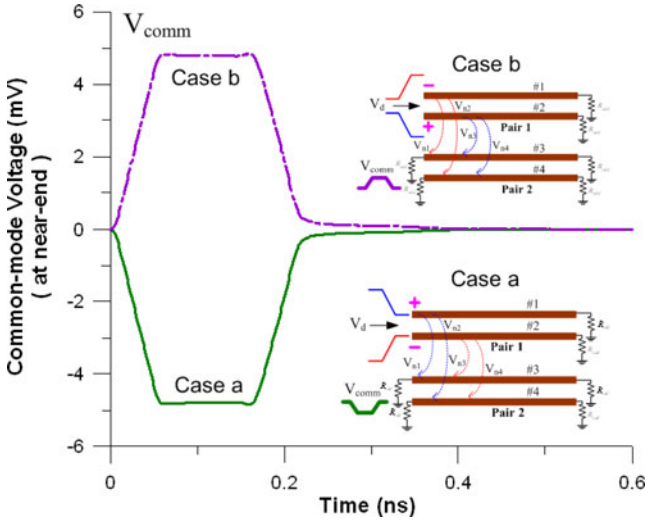

Fig. 9. Comparison of near-end common-mode noises induced between two differential pairs with two different driving signals cases.

$$V_f \approx -V_i \frac{T_d}{t_r} \times k_{\text{far}} = -V_i \times \frac{T_d}{2t_r}\left(\frac{L_m}{L_s} - \frac{C_m}{C_s + C_m}\right) \tag{9}$$

where *L* and *C* are the inductance and capacitance, and subscripts *s* and *m* indicate self and mutual terms, respectively, T_d is the line delay time, and k_{near} and k_{far} are the near- and far-end crosstalk coefficients, respectively.

Since the near-end crosstalk is evident at the receiving end of a differential serpentine delay line, but far-end crosstalk appears at the driving end [3], the common-mode noise that is induced by the crosstalk effect at the receiving end of a differential serpentine delay line should be considered in investigating the near-end crosstalk noise. Moreover, because the signals that propagate on differential lines alternate between positive and negative, the coupling between two differential pairs can be divided into two kinds—a and b, as shown in Fig. 9. The near-end common-mode voltage, which is the common-mode voltage at the near-end of parallel traces, can be approximated by

$$V_{\text{common}} = \frac{\left(\sum_{i=1}^{4} V_{\text{ni}}\right)}{2} \tag{10}$$

where V_{ni} denotes the near-end crosstalk noise that is induced by the adjacent traces of differential pairs, as shown in Fig. 9. For the same parameters as in the previous example in Section II, Fig. 9 compares the near-end common-mode noise waveforms for cases a and b. The two couplings, with different driving excitations of two differential trace pairs, both appear in the serpentine delay line and result in different voltage polarity but equal amplitude. Table II shows the maximum voltage levels of the near-end common-mode noises obtained by HSPICE simulation and the aforementioned formula. Clearly, the agreement between the HSPICE simulation and (10) is strong.

In Fig. 4, the common-mode noise at positions c, d, and e of the differential serpentine line has a flat dc voltage component but do not appear at the receiving end. The flat dc voltage

TABLE II
COMPARISON OF MAXIMUM VOLTAGE LEVELS OF THE NEAR-END COMMON-MODE NOISES BETWEEN HSPICE SIMULATION AND APPROACH FORMULA

V_{common} (mV)	Case a/b
HSPICE Simulation	-4.795 / 4.795
Approach Formula (14)	-4.785 / 4.785

component of common-mode noise is similar to the near-end common-mode voltage, as shown in Fig. 9. Therefore, a popular graphical method that is based on wave tracing to illustrate and predict the crosstalk waveforms of two coupled transmission lines with matched termination has been proposed [14]. The graphical method is used to elucidate the near-end common-mode noise for a differential serpentine delay line as follows. In the following illustration, the rise time is smaller than double the delay time $T_{d,p}$. Additionally, to facilitate the description, $V_{n,\mathrm{common1}}$ and $V'_{n,\mathrm{common1}}$ represent the first and second near-end common-mode noise crosstalk couplings, respectively. The terms $V_{n,\mathrm{common2}}$ and $V'_{n,\mathrm{common2}}$ represent the two near-end common-mode noise that is induced by the driving method associated with coupling case b for different differential pairs.

Consider a differential-ramped step pulse, as in the case a driving method, which propagates down the left end of differential pair 1 of a differential serpentine delay line, as shown in Fig. 10(a). Backward propagating common-mode noise crosstalk $V_{n,\mathrm{common1}}$ with negative polarity is immediately induced on the left end of differential pair 2, as shown in Fig. 10(a). After time $T_{d,p}$, $V_{n,\mathrm{common1}}$ propagates through the vertical-turn-coupled traces to near the right end of differential pair 3. Simultaneously, the differential sources arrive at the right end of differential pair 1, as shown in Fig. 10(b). At time $T_{d,p} + T_{d,vt}$, as shown in Fig. 10(c), the differential sources arrive at the right end of differential pair 2 and the driving method changes from case a to case b owing to the serpentine routing. Additionally, the two near-end common-mode noises, $V'_{n,\mathrm{common1}}$ and $V_{n,\mathrm{common2}}$, with negative and positive polarities at the right end of differential pair 1 and 3, respectively, are immediately induced by the differential sources with the case b driving method, as shown in Fig. 10(c). During the period $(T_{d,p} + T_{d,vt})$–$(1.5T_{d,p} + T_{d,vt})$, the $V'_{n,\mathrm{common1}}$ propagates through the vertical-turn-coupled traces toward the left end of differential pair 2. Simultaneously, the two near-end common-mode noises, $V_{n,\mathrm{common2}}$ and $V_{n,\mathrm{common1}}$, with different voltage polarities cancel out, as shown in Fig. 10(d). Then, when the differential sources propagate through the vertical-turn-coupled traces and reach the left end of differential pair 3, the method for driving the differential sources has already changed from case b to case a. The near-end common-mode noise $V'_{n,\mathrm{common2}}$ is immediately induced by the differential sources. At that time, the $V'_{n,\mathrm{common1}}$ arrives at the left end of differential pair 2, as shown in Fig. 10(e). After the time $2T_{d,p} + 2T_{d,vt}$, the two near-end common-mode noises, $V'_{n,\mathrm{common2}}$ and $V'_{n,\mathrm{common1}}$, with different voltage polarities cancel out, as shown in Fig. 10(f).

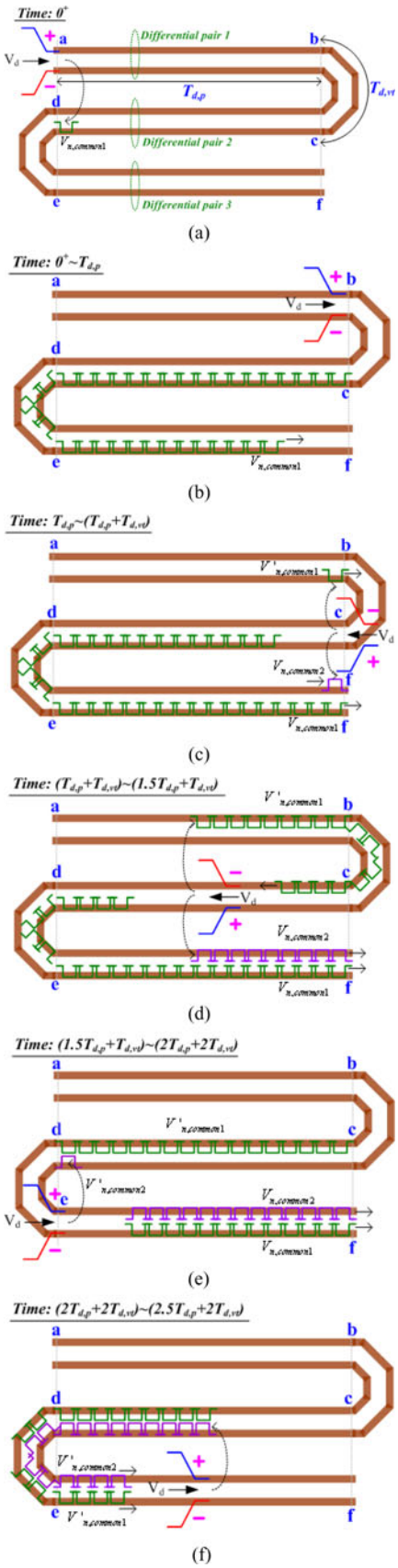

Fig. 10. Summary for generation mechanism of the near-end common-mode noises: at time (a) $t = 0^+$, (b) $t = 0^+ - T_{d,p}$, (c) $t = T_{d,p} - (T_{d,p} + T_{d,vt})$, (d) $t = (T_{d,p} + T_{d,vt})$–$(1.5T_{d,p} + T_{d,vt})$, (e) $(1.5T_{d,p} + T_{d,vt})$–$(2T_{d,p} + 2T_{d,vt})$, and (f) $(2T_{d,p} + 2T_{d,vt})$–$(2.5T_{d,p} + 2T_{d,vt})$.

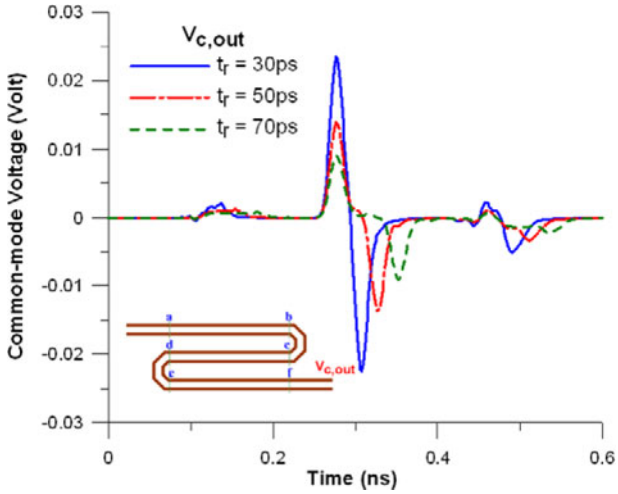

Fig. 11. Comparison of the common-mode noises at receiving end of a differential serpentine delay line with different rise times.

Owing to the symmetry of differential serpentine delay line, the two near-end common-mode noises cancel out. Therefore, the near-end common-mode noise that some or most of it is present in the interior of differential serpentine delay line but not at receiving end. Moreover, according to aforementioned graphical illustration, the existence of most of the dc voltage component in the common-mode noises at positions c, d, and e on the differential serpentine line can be explained. For example $V_{c,d}$, according to the aforementioned illustration, can be detected for the near-end common-mode noise during the period 0–$(1.5T_{d,p} + T_{d,vt})$.

IV. More Analysis of Parameters for Common-Mode Noise

Given the same parameters of cross-sectional view as used in the previous example in Section II, the differential serpentine delay line is analyzed with different parameters and conditions.

A. Rise Time Effect

Fig. 11 presents the common-mode noises at the receiving end of a differential serpentine delay line ($N = 3$) for various rise times. According to the analyses in the preceding section, the two peak voltages of common-mode noise are generated by the two ramps of the differential sources with opposite polarities. Therefore, a small rise time t_r is associated with a large common-mode noise.

B. Number of Section Effect for Inequivalent Total Length

Figs. 12(a) and 11(b) show the common-mode noises at the receiving end and the differential-to-common mode conversions ($|S_{c2d1}|$) of the differential serpentine delay line, respectively, with different number of sections N. A symmetrical structure and an odd number of sections minimize the common-mode noise of a differential serpentine delay line. However, for $N = 4$, the common-mode noise consists of mostly a negative near-end common-mode voltage and a large peak voltage, as

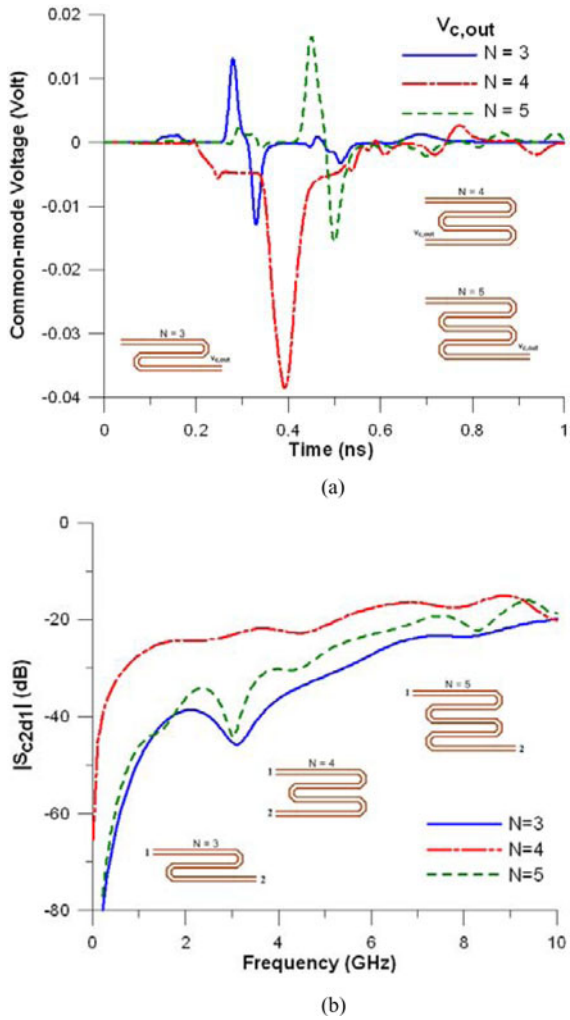

Fig. 12. Comparison of the (a) common-mode noises at receiving end and (b) differential-to-common mode conversions of the differential serpentine delay line with different numbers of section N.

shown in Fig. 12(a). For an even number of sections (such as $N = 4$), the structure is short of the vertical-turn-coupled traces to compensate for the mismatch between trace lengths, so significant common-mode noise is excited. The large negative peak common-mode voltage, which is excited by the total trace length mismatch, as shown in Fig. 12, is similar to the voltage $V_{c,d}$ in Fig. 6. Furthermore, according to the previous graphical illustration, the mechanism of common-mode noise generation for a differential serpentine delay line with $N = 4$ at the last differential pair is similar to that under the condition in Fig. 10(e) without the differential pair 3 or the left vertical-turn-coupled traces. Therefore, $V_{n,\mathrm{common}}$ propagates toward the receiving end and cannot be canceled.

For an even number of sections, the differential serpentine delay line has a large common-mode noise at its receiving end. The large common-mode noise is composed of mostly a flat near-end common-mode voltage and a large negative voltage peak, which is produced by mismatch between the lengths of the vertical-turn-coupled traces, and is similar to $V_{c,c}$ in Fig. 6. Moreover, with reference to frequency domain, as shown in

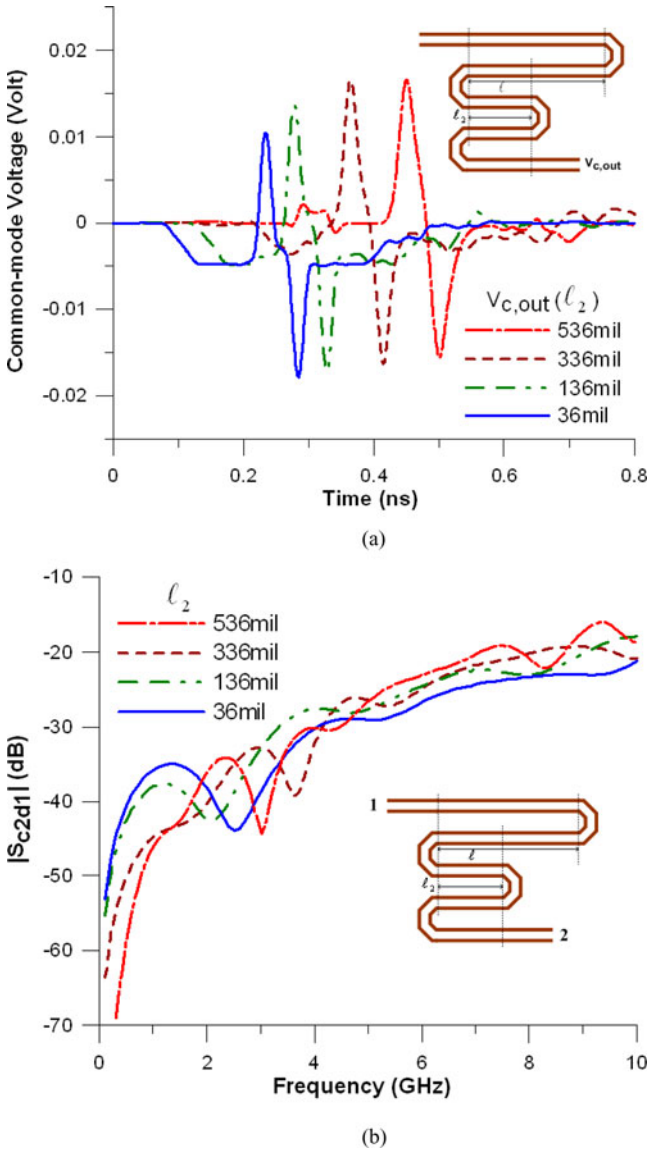

Fig. 13. Comparison of the (a) common-mode noises at receiving end and (b) differential-to-common mode conversions of the differential serpentine delay line with different lengths of parallel differential pairs.

Fig. 12(b), when the number of sections is even, such that a total length mismatch exists, the common-mode noise at the receiving end exceeds that with an odd number of sections throughout the frequency range of interest (0.1 kHz–10 GHz). The common-mode noise in the $N = 5$ case exceeds than in the $N = 3$ case. As an important design guideline, the number of sections of a differential serpentine delay line must be odd to ensure total length matching.

C. Asymmetry Effect

A routing scheme with various section lengths for a differential serpentine delay line is usually used in an industrial PCB because of spatial constraints. Figs. 13(a) and 12(b) compare the common-mode noises at the receiving end and the differential-to-common mode conversion ($|S_{c2d1}|$) of the differential serpentine delay line, respectively, with various lengths ℓ_2 of the parallel differential pair. The time-domain results in Fig. 13(a) clearly reveal that longer sections correspond to a larger peak voltage of the common-mode noise. A smaller section length corresponds to a higher near-end common-mode voltage. Its width increases but the voltage peak decreases. Based on the graphical illustration in Section III, the existence of both short and long differential pair sections in a differential serpentine delay line causes near-end common-mode noise cancellation to be incomplete. Therefore, near-end common-mode noise appears at the receiving end. As determined with reference to the frequency domain, in Fig. 13(b), a smaller section length corresponds to a large magnitude at low frequencies owing to the existence of near-end common-mode noise, which is shown in Fig. 13(a). However, the larger section length ℓ corresponds to a larger magnitude at high frequencies owing to the large voltage peak of the common-mode noise, which is also shown in Fig. 13(a). Furthermore, it indicates that the long differential lines between dual back-to-back vertical-turn-coupled traces can result in a large voltage peak of the common-mode noise, such as $V_{c,e}$ in Fig. 7.

D. Stripline Structure

The velocities of the even-mode and odd-mode signals are well known to be almost equal in a stripline structure of a homogeneous material [11], [15]. Therefore, the dual back-to-back vertical-turn-coupled traces should compensate for length mismatch in a stripline structure. The common-mode noise then becomes very small and is not an issue. However, the crosstalk effect in an asymmetrical routing of a differential serpentine delay line in the stripline, as in Fig. 14, should be investigated. Consider a differential serpentine delay stripline with a cross-sectional view as presented in Fig. 14(a) with $W = 5$ mil, $S = 9.5$ mil, $H_1 = 30$ mil, $H_2 = 8.5$ mil, $D = 15$ mil, $x = 1.5$ mil, $\varepsilon_r = 4.4$, loss tangent $= 0.02$, $N = 5$, and $\ell = 536$ mil. As in the aforementioned methods in Section II, the equivalent circuit model parameters are extracted. Based on the differential driving sources and HSPICE circuit model method that was described in the previous section, Figs. 14(a) and 13(b) compare the time-domain common-mode noises at the receiving end and the differential-to-common mode conversions of the asymmetrical differential serpentine delay line, respectively, for different lengthsℓ_2. Additionally, Fig. 14(a) shows the common-mode noises for a symmetrical differential serpentine delay line with length $\ell = 336$ and 536 mil. In Fig. 14(a), the large voltage peaks of common-mode noise caused by the different velocities of the even-mode and odd-mode signals in the microstrip line are not present in the stripline structure. The maximum magnitude, about -1.8 mV, of common-mode noise is low and almost the same for lengths$\ell = 336$ and 536 mil. From Fig. 14(b), the differential-to-common mode conversions for lengths$\ell = 336$ and 536 mil are both very small below 8 GHz. Accordingly, the dual back-to-back vertical-turn-coupled traces in a differential serpentine delay line can almost compensate for the length mismatch in the stripline structure.

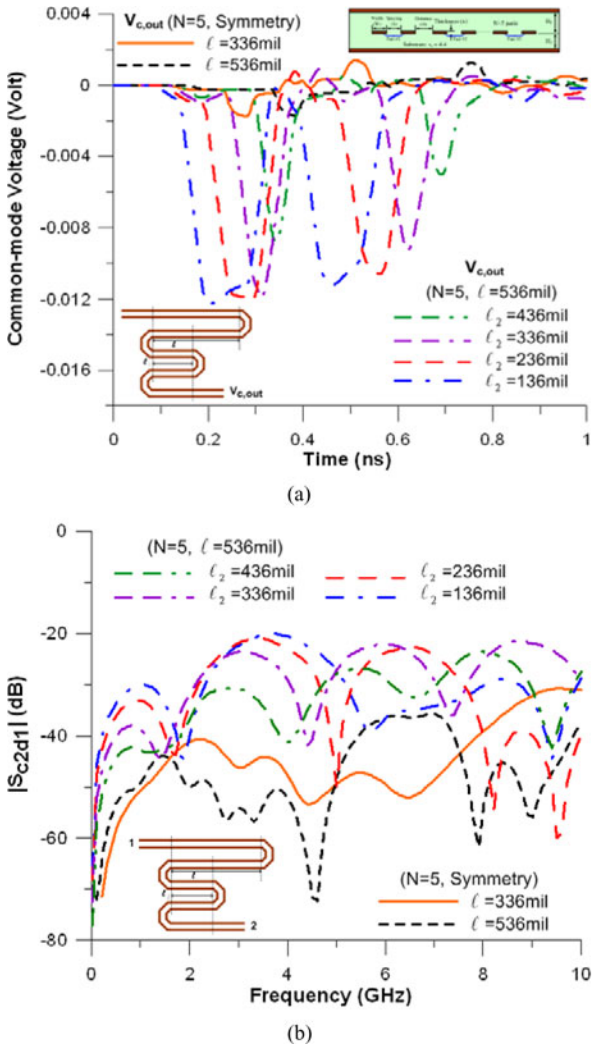

Fig. 14. Comparison of the (a) common-mode noises at receiving end and (b) differential-to-common mode conversions of the differential serpentine delay line with different lengths of parallel differential pairs.

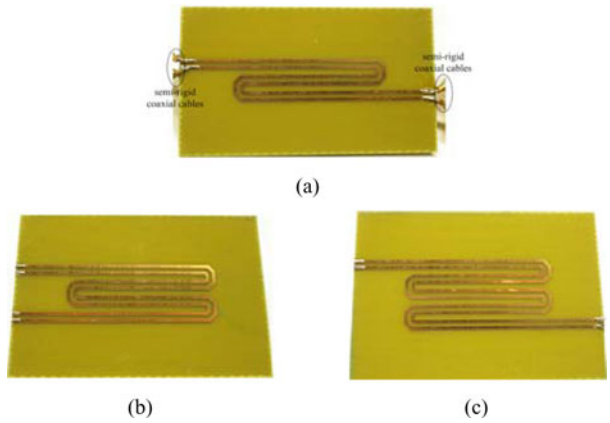

Fig. 15. Measured boards. (a) $N = 3$. (b) $N = 4$. (c) $N = 5$.

Based on the investigations in Section III, the mechanisms of generation of common-mode noise in a differential serpentine delay line involve not only length mismatch but also crosstalk. In the analysis of an asymmetrical pattern in Fig. 13(a), since the cancellation of near-end common-mode noise is incomplete, near-end common-mode noise is present at the receiving end of the asymmetrical differential serpentine delay line, as shown in Fig. 14(a). The near-end common-mode noise does not saturate between section lengths ℓ_2 of 536 and 336 mil. Hence, in this range, a longer section corresponds to larger near-end common-mode noise. When the section length exceeds 336 mil, the near-end common-mode noise becomes saturated. Additionally, with respect to differential-to-common mode conversion, as shown in Fig. 14(b), a smaller section length ℓ_2 corresponds to a larger magnitude of S_{c2d1} that is below 5 GHz. As the section length ℓ_2 is changed form 536 to 436 mil, the magnitude of S_{c2d1} becomes large. Consequently, although the dual back-to-back vertical-turn-coupled traces of the differential serpentine delay line can almost compensate for length mismatch in a stripline structure, the design guideline for minimizing common-mode noise is to maintain a symmetrical routing pattern, meaning that the parallel traces of a differential serpentine delay line have the same length.

Hence, symmetrical routing is required for a differential serpentine delay line not only with a microstrip structure but also with a stripline structure, because the near-end common-mode noise cancellation mechanism will only then be complete.

Based on the aforementioned results, the following important design guidelines to minimize the common-mode noise at the receiving end of a differential serpentine delay microstrip line are proposed. 1) The parallel traces should be short; 2) routing should be symmetrical: all parallel traces should have the same length; and 3) the number of sections must be odd: the lengths of the two traces of a differential serpentine delay line must be equal. Moreover, the routing pattern of differential serpentine delay line in a stripline structure must be symmetrical. The length between the dual vertical-turn-coupled traces is not important.

V. Experimental Validation

To verify the results of the analysis in Sections III and IV, the simulated and measured results concerning the TDT common-mode noises and the frequency-domain differential-to-common mode conversions are compared. For ease of implementation in our laboratory, the measured boards are fabricated on a millimeter scale. The differential serpentine delay line has a cross section with $W = 0.6$ mm, $S = 0.6$ mm, $D = 1.05$ mm, $x = 0.035$ mm, $H = 0.4$ mm, a substrate material with $\varepsilon_r = 4.4$, and loss tangent $= 0.02$. The length of the pairs of the parallel differential serpentine delay line is 23 mm and the considered numbers of sections N are 3, 4, and 5. The photographs of the measured boards are shown in Fig. 14. As in the aforementioned methods in Sections II, the equivalent circuit model parameters are extracted. A time-domain reflectometer TEK/CSA8000 and a frequency-domain network analyzer Agilent/E5071B are adopted to verify the experimental results. With both the source resistance and the load resistance at 50 Ω, the launching voltage source is drawn out of the reflectometer in the HSPICE simulation.

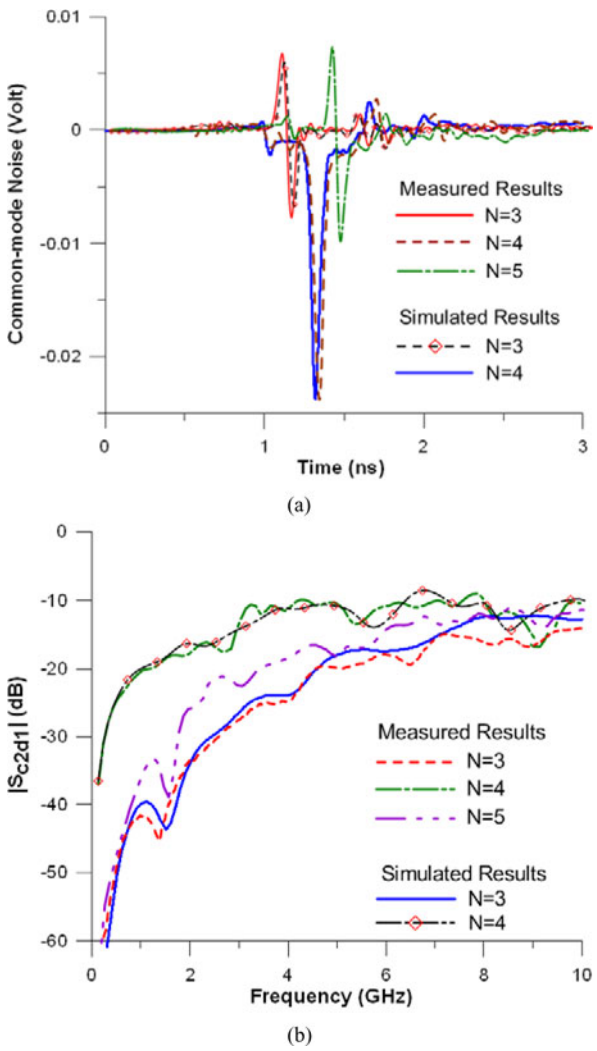

Fig. 16. Comparison of the (a) common-mode noises at receiving end and (b) differential-to-common mode conversions of the differential serpentine delay line with different lengths of parallel differential pairs.

Figs. 16(a) and 15(b) compare the simulated and measured time-domain common-mode noises at the receiving end and the frequency-domain differential-to-common mode conversions (S_{c2d1}) of the differential serpentine delay line, respectively, for various numbers of sections, respectively. The results of the simulation agree closely with the measurements, as shown in Fig. 16(a). Furthermore, a comparison with Fig. 16(b) indicates that the simulated differential-to-common-mode noise conversions agree closely with are consistent with the measured ones. However, most of the deviations between the HFSS simulations and the measurements are attributable to neglect of the semirigid coaxial cable, some small variations in the properties of the fabricated material (such as dielectric constant, loss tangent), and the definition of the port(s), among others factors. Although a slight discrepancy exists, the results obtained using the qualitative model, by quantitative analysis, by simulation, and by measurement, all verify the effect and existence of common-mode noise at the receiving end of a differential serpentine delay line.

VI. Conclusion

The mechanisms of generation of transient transmission common-mode noise in the differential serpentine delay line under weak coupling condition are investigated. A transient waveform analysis based on a simulation using HSPICE and mixed-mode *S*-parameters using the differential-to-common mode conversion S_{c2d1} that was obtained by simulation using HFSS for a differential serpentine delay line is performed to study the mechanisms of common-mode noise generation. The three main generation mechanisms are the mismatch of the lengths of vertical-turn-coupled traces, the effect of the length of parallel-coupled traces, and the crosstalk noise effect. A graphical method based on wave tracing was presented to illustrate the mechanism of near-end common-mode noise cancellation for a differential serpentine delay line with symmetry. According to some investigations of practical, commonly used layout routings performed, the following important design guidelines for minimizing common-mode noise at the receiving end of a differential serpentine delay microstrip line are proposed: 1) the parallel traces should be short; (2) the routing scheme should be symmetrical; (3) the number of sections must be odd. Additionally, for a stripline structure, the routing pattern of a differential serpentine delay line must remain symmetrical. The length between dual vertical-turn-coupled traces is not important. Consequently, a symmetrical routing pattern, in which the parallel traces of the differential serpentine delay line are of equal length, is required not only in a microstrip structure but also in a stripline structure, because only then can the near-end common-mode noise be completely cancelled. A comparison between the simulated and measured results validated the equivalent circuit model and analytical approach.

Acknowledgment

The authors would like to thank NTUEE EDAPS Lab and Ansoft Taiwan for providing the measurement equipment and simulation software. They would also like to thank V. Hung, C.-F. Hung, J. Wu, and B. Wei for providing helpful information and the reviewers for the helpful suggestions.

References

[1] E. Bogatin, *Signal Integrity-Simplified* (Hall Modern Semiconductor Design Series' Sub Series: PH Signal Integrity Library). Englewood Cliffs, NJ: Prentice-Hall, 2003.

[2] R. B. Wu and F. L. Chao, "Laddering wave in serpentine delay line," *IEEE Trans. Compon., Packag., Manuf. Technol., B*, vol. 18, no. 4, pp. 644–650, Nov. 1995.

[3] W. D. Guo, G. H. Shiue, and R. B. Wu, "Comparison between serpentine and flat spiral delay lines on transient reflection/transmission waveforms and eye diagrams," *IEEE Trans. Microw. Theory Tech.*, vol. 54, no. 4, pp. 1379–1387, Apr. 2006.

[4] G. Kim, J. Kim, S. Lee, J. Kim, and J. Kim, "Mode-impedance method for modeling and analysis of crosstalk in differential meander delay lines," in *Proc. IEEE Electric. Design Adv. Packag. Syst. Symp.*, Dec., 2008, pp. 93–96.

[5] C. R. Paul, *Introduction to Electromagnetic Compatibility*, 2nd ed. York: Wiley, 2006.

[6] W. Fan, A. Lu, L. L. Wai, and B. K. Lok, "Characteristics of phase-delay time on meander differential signal lines and shielded meander differential signal line," in *Proc. 18th Int. Zurich Symp. Elecromagn. Compat.*, Dec. 2007, pp. 217–220.

[7] CST Microwave Studio Manual Computer Simulation Technology, Germany. (2003). [Online]. Available: http://www.cst.com.
[8] W. Fan, A. Lu, L. L. Wai, and B. K. Lok, "Mixed-mode S-parameter characterization of differential structures," in *Proc. IEEE 5th Electron. Packag. Technol. Conf.*, Dec., 2003, pp. 533–537.
[9] High Frequency Structure Simulator. ver. 12, Ansoft, Pittsburgh, PA. (2009). [Online]. Available: www.ansoft.com.
[10] P. Harms and R. Mittra, "Equivalent circuits for multiconductor microstrip bend discontinuities," *IEEE Trans. Microw. Theory Tech.*, vol. 41, no. 1, pp. 62–69, Jan. 1993.
[11] G.-H. Shiue, W.-D. Guo, C.-M. Lin, and R.-B. Wu, "Noise reduction using compensation capacitance for bend discontinuities of differential transmission lines," *IEEE Trans. Adv. Packag.*, vol. 29, no. 3, pp. 560–569, Aug. 2006.
[12] G. H. Shiue and R. B. Wu, "Reduction in reflections and ground bounce for signal line through a slotted power plane by using differential coupled microstrip lines," *IEEE Trans. Adv. Packag.*, vol. 32, no. 3, pp. 581–588, Aug. 2009.
[13] C. R. Paul, "Solution of the transmission-line equations under the weak-coupling assumption," *IEEE Trans. Electromagn. Compat.*, vol. 44, no. 3, pp. 413–423, Aug. 2002.
[14] S. H. Hall and H. L. Heck, *Advanced Signal Integrity for High-Speed Digital System Design*. Hoboken, NJ: Wiley, 2009, ch. 4.
[15] Y. S. Cheng, W. D. Guo, G. H. Shiue, H. H. Cheng, C. C. Wang, and R. B. Wu, "Fewest vias design for microstrip guard trace by using overlying dielectric," in *Proc. IEEEElect. Performance Electron. Packag.*, San Jose, CA, Oct. 27–29, 2008, pp. 321–324.

Guang-Hwa Shiue (M'07) was born in Tainan, Taiwan. He received the M.S. degree in electrical engineering from the National Taiwan University of Science and Technology, Taipei, Taiwan, and the Ph.D. degree in communication engineering from National Taiwan University, Taipei, in 1997 and 2006, respectively.

In 1999, he joined the faculty of the Department of Electronic Engineering, Chin Min Institute of Technology, where he was a Lecturer. In 2001, he joined the faculty of the Department of Electronic Engineering, Jinwen University of Science and Technology, where he was a Lecturer from 2001 to 2006 and an Assistant Professor during 2006–2008. In 2008, he joined the faculty of the Department of Electronic Engineering, Chung Yuan Christian University, Taipei, where he is currently an Assistant Professor. His research interests include numerical electromagnetic field, microwave planar circuits, signal/power integrity for high-speed digital systems, electromagnetic interference/compatibility for high-speed/frequency electronic systems, and electrical characterization of system-in-package.

Jia-Hung Shiu was born in Changhua, Taiwan, in 1987. He received the B.S. degree in electrical engineering form Chung Yuan Christian University, Taoyuan, Taiwan, in 2009, where he is currently working toward the M.S. degree in communication engineering.

His current research interests include signal integrity and electromagnetic compatibility for high-speed digital circuits.

Yi-Chin Tsai was born in Pingtung, Taiwan, in 1988. She received the B.S. degree in engineering and management of advanced technology from Chang Jung Christian University, Tainan, Taiwan, in 2010. She is currently working toward the M.S. degree in communication engineering at Chung Yuan Christian University, Taoyuan, Taiwan.

Her research interests include signal integrity and electromagnetic compatibility for high-speed digital circuits.

Che-Ming Hsu was born in Taoyuan, Taiwan, in 1987. He received the B.S. degree in electrical engineering from Chung Yuan Christian University, Taoyuan, Taiwan, in 2010, where he is currently working toward the M.S. degree in communication engineering.

His research interests include signal/power integrity and electromagnetic compatibility design for high-speed digital circuits.